PAPER

Check for updates
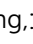
Enhanced regeneration of bone defects using sintered porous Ti6Al4V scaffolds incorporated with mesenchymal stem cells and platelet-rich plasma†

Ji Li, [ID] ‡[a] Ketao Wang,‡[ab] Xiaowei Bai,[a] Qi Wang,[a] Ningyu Lv[a] and Zhongli Li*[a]

A new highly controlled powder sintering technique was used for the fabrication of a porous Ti6Al4V scaffold. The platelet-rich plasma (PRP) was prepared using whole blood. The PRP was used as a cell carrier to inject bone marrow mesenchymal stem cells (MSC) into the pores of the Ti6Al4V scaffold in the presence of calcium chloride and thrombin, and then the composite construct of porous Ti6Al4V loaded with PRP gel and MSC was obtained. The bare Ti6Al4V scaffold and the Ti6Al4V scaffold loaded with MSC were used as controls. The characteristics and mechanical properties of the scaffold, and the biological properties of the constructs were evaluated by a series of *in vitro* and *in vivo* experiments. The results show that the sintered porous Ti6Al4V has good biocompatibility, and high porosity and large pore size, which can provide sufficient space and sufficient mechanical support for the growth of cells and bones without an obvious stress shielding effect. However, Ti6Al4V/MSC/PRP showed a significantly higher cell proliferation rate, faster bone growth speed, more bone ingrowth, and higher interfacial strength. Therefore, the porous Ti6Al4V scaffolds incorporated with MSC and PRP may be more effective at enhancing bone regeneration, and is expected to be used for bone defect repair.

1. Introductions

Bone regeneration and reconstruction remain a challenging topic in the clinic and bone tissue engineering.[1,2] Various studies have been performed for developing materials that can replace autogenous bones, but most of them have shown very limited capability.[3] In recent years, porous Ti6Al4V has attracted much attention due to its excellent performance.[4] The porosity results in a relatively low elastic modulus and then reduce the stiffness mismatch between the implant and bone, which may ameliorate bone resorption due to stress shielding.[5,6] Besides, the porous structure could mimic the extracellular matrix to provide space for angiogenesis and cell ingrowth with sufficient mechanical support.[6–8] However, insufficient bone regeneration of porous Ti6Al4V leads to the bone not joining even when using mechanical supports for large bone defects.[9] Tissue engineering strategies for bone regeneration and reconstruction endeavor to create alternative but functional constructs to guide new bone

formation.[10] To obtain good osseointegration, four elements were necessary for the implants: structural integrity; an osteo-conductive structure that allow bone ingrowth; osteogenic cells with the potential of differentiation and proliferation; and osteoinductive factors that induce the bone regeneration and repair.[11] Therefore, to further enhance the osteogenesis ability, it is necessary to introduce osteogenic cells and bioactive molecules into the porous Ti6Al4V.[8]

Bone regeneration requires osteogenic cells to lay down a protein and mineralized matrix upon a scaffold or template when provided with the proper biological cues.[12] Bone marrow mesenchymal stem cell (MSC) usually harvested from the bone marrow is the most common type of cell for this application. MSC has the potential of multi-differentiation.[13,14] Osteogenic differentiation of MSC is regulated by is regulated by various extracellular factors.[15] Platelet-rich plasma (PRP) is a fraction of plasma with a high concentration of platelets which is usually prepared from whole blood.[16] Once activated by thrombin or calcium chloride ($CaCl_2$), the liquid PRP will clot and formed PRP gel because of the amount of fibrinogens.[17] Unlike the previous hydrogels (*e.g.* collagen, fibrin, alginate),[18] PRP gel can release a large proportion of biologically active growth factors, such as platelet-derived growth factor (PDGF), basic fibroblast growth factor (bFGF), transforming growth factor-β (TGF-β), insulin-like growth factor (IGF) *etc.*, and these cytokines are known to regulate the proliferation and osteogenesis of MSC,

[a]*Department of Orthopedics, General Hospital of PLA, No. 28 Fuxing Road, Haidian District, Beijing 100853, China. E-mail: lizhongli@263.net; Fax: +86 10 66938306; Tel: +86 10 66938306*

[b]*Department of Orthopedic Surgery, Zhongshan Hospital, Fudan University, Shanghai, China*

and promote newly bone formation.[19,20] Additionally, the isolated single cells can be easily suspended during the gelation process of PRP, and the fibrin network will provide a three-dimensional (3D) cell distribution throughout the whole construct and maintain cell phenotype.[21,22] Thus, PRP gel can be used as cell carrier for the migration, proliferation, and differentiation of MSC.[23] However, PRP gel often lacks the mechanical properties necessary for load-bearing applications.[24,25]

In the present work, we aim to obtain a composite functional construct to enhance bone regeneration and reduce healing time. A new highly controlled powder sintering technique was used for the fabrication of porous Ti6Al4V scaffold with high porosity, large pores and excellent mechanical properties. The PRP was prepared using human whole blood by two-step centrifugation procedure. The PRP containing a large amount of growth factors was used as a cell carrier to inject bone marrow mesenchymal stem cell (MSC) into pores of the Ti6Al4V scaffold in the presence of calcium chloride and thrombin, and then the composite construct of porous Ti6Al4V loaded with PRP gel and MSCs can be implanted into defect area. We investigated whether the porous MSC/PRP/Ti6Al4V scaffold construct enhanced the osseointegration *in vitro* and *in vivo*.

2. Materials and methods

2.1 Preparation of porous scaffold

Porous Ti6Al4V scaffold was prepared as previously described using Ti6Al4V powder as the starting material.[26] In brief, Ti6Al4V, H_2O, agar, Tergitol TMN, triton and ammonium alginate with a certain proportion were used to prepare a powder suspension and then mixed to obtain a fluid foam. The foam was moulded and then dried at atmospheric pressure and room temperature to obtain a green artifact. The artifact was first calcined with a slow heating step (<20 °C per hour) to 400–600 °C under Ar atmosphere and constant temperature for 2 h, and then, it was sintered with slow heating to 1250 °C under vacuum and constant temperature for 2 h.

Then the porous Ti6Al4V material was cut into specimens with different types. Rod specimens of ϕ 10 × 20 mm in length and ϕ 4 × 10 mm in length, disc specimens of δ 3 mm × ϕ 10 mm were prepared for different tests. Ultrasonic cleaning and sterilizing of all samples, before the tests.

2.2 Characterizations of the scaffold

Although some characterizations of the porous scaffold have been reported in our previous study,[27–29] slight differences in different batches still existed. Thus, the 10 × 20 mm samples were characterized in a standard process in the present work to ensure the accuracy of the study and the success fabrication of the porous structure. In brief, surface topography of the sample was examined by an optical microscope. Micro-CT and scanning electron microscopy (SEM) were used to determine the mechanical integrity and measure the pore size of the scaffold. Porosity was calculated by bulk density and apparent density. An axial compression test was used to measure the stiffness, compressive strength and elastic modulus of the samples.

2.3 Preparation of PRP and determination of growth factors

This study was approved by the institutional ethical review board of the People's Liberation Army General Hospital (PLAGH), and informed consent was obtained from all patients. Whole blood samples were obtained from 8 donors with an average age of 39.3 ± 5.8 years old. All samples were used to prepare PRP individually instead of in a pooled manner. A double centrifugation process was involved in PRP preparation as previously described.[24] Briefly, 19 ml of whole blood were drawn from the antecubital vein in a disposable blood bag containing 1 ml of ethylenediamine tetra-acetate (EDTA) as an anticoagulant. 0.5 ml blood was drawn from each sample for a complete blood count, and the rest of the blood sample was centrifuged at 300g for 10 minutes, separating the volume into three phases: platelet-poor plasma, PRP, and red cells. The upper two phases were transferred to a new tube for a second centrifugation at 1200g for 20 minutes. After that, approximately 1–2 ml of volume at the bottom was reserved, while the upper 85% phase was discarded. The platelet concentration and the residual number of leucocytes in the PRP were determined with a cytoanalyzer. Different volumes of plasma in the upper phase were added to create PRP with concentrations of about 1500×10^9 platelets (pl) per L. Serum was considered PRP with 0×10^9 pl per L. Centrifugation was performed at room temperature.

Then the level of growth factors of PRP were determined by enzyme-linked immunosorbent assay (ELISA). PRP was activated with activating solution (bovine thrombin (Gibco, 1000 IU ml^{-1}) and 10% $CaCl_2$) in the ratio of 9 : 1 (v/v) and the resulting solution was incubated at 37 °C for 1 hour. Then, the formed gel was mashed and centrifuged at 3000g for 10 minutes in order to remove debris and collect the supernatant. All the supernatants were collected and frozen at 80 °C until use. Human TGF-β1, PDGF-AB, IGF1, and bFGF concentrations in supernatants and in whole blood were determined according to the reagent protocols of the quantitative ELISA kits (R&D Systems, Minneapolis). Optical density was determined at 450 nm as previously reported.[30]

2.4 Cell culture and identification

Human MSCs were obtained from bone marrow according to a previous protocol.[31] Briefly, 4 ml fresh bone marrow was obtained from the iliac crests of the 8 donors. All bone marrow samples were used to culture and identify MSC individually instead of in a pooled manner. Phosphate buffered saline (PBS) was used to wash the samples twice and then brought them up to 6 ml. 4 ml of lymphocyte separation medium and the 6 ml samples were poured gently into a 10 ml centrifuge tube. The samples were separated into three phases after centrifugation at 900g for 20 minutes. The middle layer was abandoned and the washed with PBS, the pellet in the bottom was resuspended and transferred in alpha-minimal essential medium (α-MEM) supplemented with 10% v/v fetal bovine serum (FBS), 100 units per ml penicillin and 100 μg ml^{-1} streptomycin and incubated at 37 °C in an atmosphere of 5% CO_2/95% air. The medium was

changed every 3 days and the cells were reseeded at a split ratio of 1 : 3. MSC were used for the *in vitro* experiments.

Tri-lineage induction of MSCs were performed according to a previously reported.[32] Briefly, the fourth passage cells were harvested and incubated in osteogenic induction medium for 14 or 28 days, adipogenic induction medium for 14 days, and chondrogenic induction medium for 28 days, respectively. Cells were incubated at 37 °C and 5% CO_2. Alkaline phosphatase (ALP) staining (on day 14) and von Kossa staining were performed to detect the osteogenesis at day 28, and Oil Red O staining was used to assess the adipogenic potency at day 14 according to the previously reported methods.[32]

Flow cytometry was used to analyze the cell surface antigen profile of MSCs according to a previous protocol. Fluorescein isothiocyanate-conjugated monoclonal antibodies against human CD73, CD105, CD45, HLA-DR, allophycocyanin-conjugated antibodies against CD90, and phycoerythrin (PE)-conjugated monoclonal antibodies against human CD31, CD44 were used. Briefly, the MSCs were washed twice and incubated with or without antibodies for 20 minutes at 4 °C. Then, all the samples were washed twice again with PBS and fixed with 0.4 ml of 1% paraformaldehyde. At last, the data were obtained by the flow cytometry and then analyzed with WinMDI 2.9 software.

2.5 *In vitro* biochemical assays

2.5.1 Groups setting. MSC at passage 4 ($\sim 2 \times 10^6$) were seeded in porous Ti6Al4V scaffolds to form MSC/Ti6Al4V constructs. MSC at passage 4 ($\sim 2 \times 10^6$) were resuspended in 1 ml of PRP (1500×10^9 pl per L), followed by loading porous Ti6Al4V (δ 3 mm $\times$ ϕ 10 mm) with MSC/PRP in the presence of a mixture of 10% $CaCl_2$ and bovine thrombin (250 U ml^{-1}) to form MSC/PRP/Ti6Al4V constructs [Fig. S1a in the ESI†]. The mixture of $CaCl_2$ and bovine thrombin was used the protocol of 1 : 9 v/v. The functions of $CaCl_2$ and thrombin were to activate the PRP and form PRP gel by initiating the coagulation mechanism and releasing growth factors from α-granules of platelets.[17,33]

2.5.2 Cell proliferation and attachment. Cell proliferation and attachment were test in a standard process. Ti6Al4V/MSC constructs and Ti6Al4V/MSC/PRP constructs were respectively placed in a 48-well plate and cultured for 4 h. Medium was added and changed every 2–3 days. After the 1, 3 and 7 days of induction, the medium was abandoned and the live/dead assay was performed using the viability kit to assess the cell viability. 300 μl of 4 μM EthD-1 and 2 μM of calcein AM in PBS per sample were added and incubated for about 40 min. Fluorescence microscopy were used to obtain images in which the green and red denote live and dead cells, respectively. Cell viability and proliferation were quantified by adding the Cell Counting Kit-8 assay (CCK-8) solution at a ratio of 100 μl ml^{-1} at the 1st, 3rd, and 7th day of cell culture, and the absorbance was measured at a wavelength of 450 nm. After culturing the cells for 7 days, the samples were washed with PBS to remove nonadherent cells and fixed with 2.5 wt% glutaraldehyde for 1 h. Dehydration was performed using a series of gradient ethanol solutions (50%, 70%, 90%, 95%, and 100%), and the pure isopentyl acetate was followed added. Cells morphology attached on the scaffold were observed by SEM after being sputter-coated with a 10 nm thick gold film.

2.5.3 Cell differentiation. The previously reported protocols for differentiation of MSCs were as a reference in the present work.[32] For osteogenic differentiation, the Ti6Al4V/MSC and Ti6Al4V/MSC/PRP constructs were incubated in 48-well cell culture dishes with growth medium (GM). The MSCs were harvested after being cultured for 7 and 14 days. The total RNA was extracted and reverse transcribed into cDNA. Expression levels of ALP, BSP, Runx-2, COL I and osteocalcin were determined by RT-PCR. The sequences of the primers are shown in Table S1 in the ESI.†

2.6 Implantation

2.6.1 Groups setting. MSC at passage 4 ($\sim 2 \times 10^6$) were resuspended in 1 ml of PRP (1500×10^9 pl per L), followed by loading porous Ti6Al4V (4×10 mm) with MSC/PRP in the presence of a mixture of 10% $CaCl_2$ and bovine thrombin (250 U ml^{-1}) to form MSC/PRP/Ti6Al4V constructs, which were used for the test group. MSCs were seeded in porous Ti6Al4V scaffolds to form MSC/Ti6Al4V constructs as the positive control group. The bare porous Ti6Al4V scaffolds were used as the blank control group. 54 New Zealand white rabbits (5–8 months and 3.3 ± 0.6 kg) were divided into three groups according to the different types of implants randomly. Among them, 27 rabbits were used for the histological analysis, and another 27 were for micro-CT and push-out tests. All surgical procedures were performed in accordance with the ARRIVE guidelines and the National Institutes of Health guide for the care and use of laboratory animals (NIH Publications no. 8023, revised 1978) and approved by our Ethics Committee.

2.6.2 Surgery procedures. After anaesthesia by the intramuscular injection, both hind limbs of each rabbit were fixed for surgery under standard sterile conditions. A straight 2–4 cm skin incision was made over the lateral femoral condyle, and then the underlying soft tissue were blunt dissected to expose the lateral femoral condyle. The dental implantation drill of $4 per mm was used to drill in lateral femoral condyle with the irrigation of sterile saline. After inserting the implant into the hole, repositioning the surrounding muscles and sewing the subcutaneous tissues and the skin. The surgery was shown in Fig. S1 in ESI.† The procedures were repeated for the contralateral limb and the rest rabbits. Antibiotics were injected into the muscles of each rabbit to prevent infection during the operation. Complications or adverse reactions were checked every day after the operation and the rabbits were allowed unrestricted cage activity.

2.6.3 Histological analysis. Sequential fluorochrome markers were used in this study to observe the bone ingrowth clearly. At 2 weeks and 3 days before 27 rabbits were sacrificed, tetracycline of 10 mg ml^{-1} and calcein green of 10 mg ml^{-1} were intramuscular injected, respectively. The 27 rabbits were sacrificed after 2, 8 and 12 weeks of surgeries (9 rabbits at every time point) by overdose injection of anesthetic solution. The femora containing implants were retrieved and trimmed (Fig. S1d†). All samples were fixed in 70% ethanol for 2 weeks, and then

dehydrated in 70–100% gradient ethanol. The dehydrated samples were embedded in methyl methacrylate solution to polymerize at 37 °C without decalcification. Cutting and grounding the samples into 20 μm transverse sections slices by the diamond saw. Then, a laser confocal microscope (Leica, Germany) were used to obtain images with fluorochrome markers, and then the bone mineralization apposition rate (MAR) was measured, which indicated the new bone growth rate.[34] After that, the sections slices were stained using toluidine blue. The BIC values, which mean the direct contact between the new bone and the implant, was measured by optical microscopy.[35] The hemorrhage, necrosis, exudation, neo-vascularization and capsule of the implanted site were evaluated in a semi quantitative way.[36]

2.6.4 Micro-CT analysis and push-out test. Another 27 rabbits were also sacrificed at 2, 8 and 12 weeks after surgeries (3 in each group at every time point). The femora were removed, and the extent of bone growth was observed by the micro-CT. After the sub-reconstruction of the micro-CT data, quantitative analysis is carried out according to the method of Butz,[37] and the bone volume was measured. After that, all samples were stored at −20 °C before the push-out testing. The samples were fixed in a special mold resin. Closed loop servo hydraulic testing machine was used to evaluate the shear strength of the bone-implant interface. The maximum push-out stress was recorded while the implants were pushed out from the bone at 1 mm min^{-1}.

2.7 Statistical analysis

The data were analyzed by Statistical Product and Service Solutions (SPSS) 23.0 software. The values are presented as the mean ± standard deviation (S.D). One-way ANOVA or Student's *t*-test are used to evaluate statistical differences, and $P < 0.05$ indicated a significant statistical difference. The graphs were drawn by SPSS or GraphPad 6.0.

3. Results

3.1 Characterizations and mechanical properties

Fig. 1 showed that the surface of the porous Ti6Al4V sample is rough. Micro-CT images showed that the inside pore distribution was irregular, but the scaffold structure was complete and continuous. The pores of different sizes and shapes were observed under scanning electron microscopy (SEM). There were no loose powder particles in the pores or interlayer differentiation. The mechanical integrity of the cell strut and the 3D connectivity were confirmed. The results of SEM showed that the average porosity of the scaffolds was about (76.13% ± 3.35)%, and the average pore size was about 523.86 ± 223.15 μM.

Based on the collected force displacement data, the compression stress/strain values were calculated and the compressive stress–strain curve was plotted. The modulus of elasticity is obtained from the slope of the curve in the linear elastic region (Fig. S2†). In this study, the average compressive modulus of elasticity is 1.87 ± 0.38 GPa, and the strength is 96.17 ± 10.13 MPa. Therefore, the samples with porosity of about 76.13% and elastic modulus of about 1.87 GPa were successfully prepared.

3.2 Platelet counts of PRP

The cytoanalyzer measurements demonstrated that the average platelet concentrations of PRP was $2064 ± 63.7 × 10^9$ L^{-1}, a more than 8.9-fold increase compared to that of whole blood ($232 ± 13.96 × 10^9$ L^{-1}, $p < 0.001$). PRPs with $1500 × 109$ L per platelets were obtained by manipulating the volume of plasma. The ELISA results of PRP released growth factors were shown in Table S2.†

3.3 Isolation and definition of human bone marrow MSCs

One week after the initial culture of MSC, the cells were observed to be spindle shaped in the monolayer (Fig. 2). The fusion rate of MSCs reached 80–90% at 2 weeks after seeding, and then they were propagated in the ratio of 1 : 2 every 2 days. ALP, Von Kossa, Oil-red-O, toluidine blue and Alcian blue staining were used to detect the ability of multi-differentiation. As shown in Fig. 2, strong ALP activity and mineralization were observed in osteogenic cultures. Besides, when MSCs were exposed to fat forming medium, there was obvious accumulation of lipid droplets. Obvious cartilage formation was observed in chondrogenesis culture. These results confirm the multi-directionality of MSCs. In addition, flow cytometry analysis
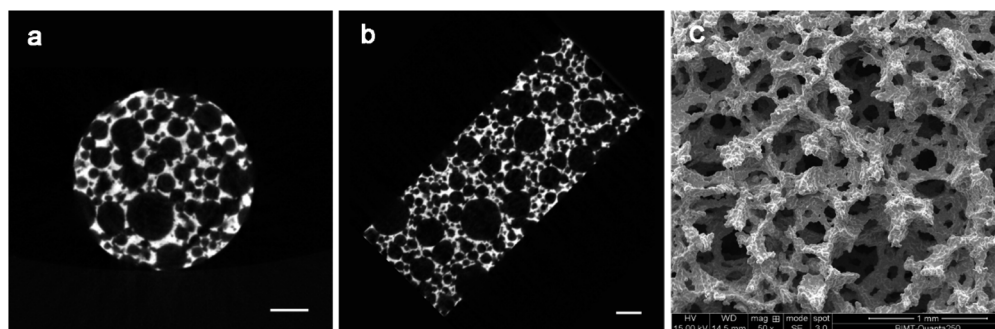

Fig. 1 Characterization of the sintered porous Ti6Al4V samples: (a) and (b) are cross-section images obtained by micro-CT; (c) is the SEM image. Scale bars in the images represent 1 mm.
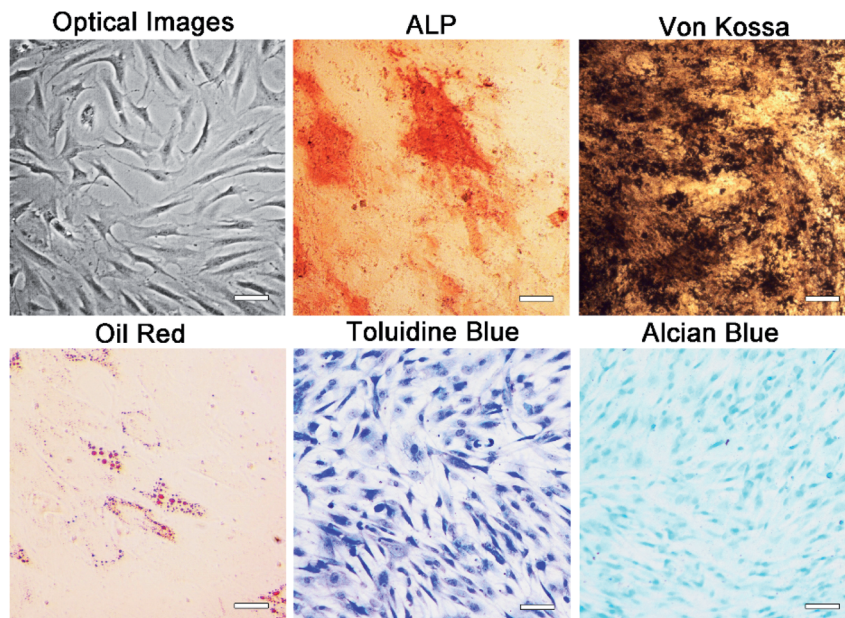
Fig. 2 Morphology and multipotency ability of MSCs: optical images and tri-lineage induction of MSCs. Scale bars in the images represent 200 μm.

showed that these cells were positive for mesenchymal cell markers, CD73 and CD105, CD90 and CD44, negative for endothelial or hematopoietic markers, CD31 and CD45 (Fig. S3†). This part of our work verifies the purity of MSCs.

3.4 *In vitro* biochemical assays

3.4.1 Cell proliferation and attachment. From the fluorescent microscope image of live/dead cell analysis in Fig. 3, it is observed that the living cells (green) are distributed on all the sample surface, while the dead cells (red) are relatively few. In general, all the samples showed good viability, and there was no significant number of dead cells at each time point. Fluorescence images showed that cell proliferation increased with

time, and the number of cells in MSC/PRP/Ti6Al4V group was significantly higher than that in the group without PRP (Fig. 3a–c and e–g).

SEM images indicated that the cells in both groups grew well on the surface of the material, while the cells proliferated faster and highly concentrated on the surface of scaffold with PRP. In addition, cells in PRP group grew from the edge into the pores and converged (Fig. 3d and h). The surface of Ti6Al4V scaffold is covered with cell materials, so it is difficult to distinguish between cells and extracellular matrix. In the CCK-8 evaluation of cell proliferation, there was significant difference in each group during the whole incubation period ($P < 0.05$), and the optical density (OD) value showed increase in both groups.
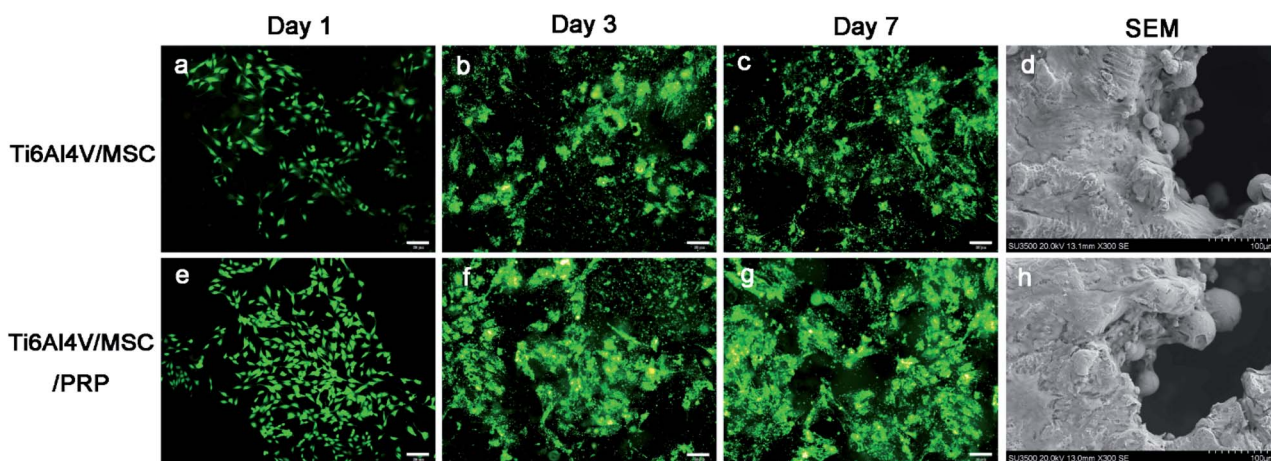

Fig. 3 Cell proliferation and live/dead fluorescence microscopy images after 1, 3 and 7 days of three groups: (a–c) Ti6Al4V/MSC group and (e–g) Ti6Al4V/MSC/PRP group; and the SEM images of cell attachment: (d) Ti6Al4V/MSC group and (h) Ti6Al4V/MSC/PRP group. Scale bars in (a–c and e–g) represent 50 μm; scale bars in (d and h) represent 100 μm.

However, the values in PRP group at each time point was significantly higher than that in the other group (Fig. 4 CCK-8). It was suggested that porous Ti6Al4V and PRP have no cytotoxic effect on MSCs, and PRP may promote the growth of MSCs.

3.4.2 Osteogenic differentiation. Without adding osteogenic agents such as ascorbic acid, dexamethasone and β-glycerophosphate, 7 days and 14 days after induction in normal GM, the expression of osteogenic proteins and marker genes was detected by qRT-PCR. In Fig. 4, quantitative evaluation results showed that Ti6Al4V/MSC/RPP group stimulated the expression of ALP, BMP-2, COL 1, OCN and RUNX 2 compared with the group without PRP ($P < 0.05$). The morphological changes of MSCs at different time points are shown in Fig. S4.† Most of the MSCs showed ovoid, pyramidal at day 7, the number of MSCs in both groups increased significantly and showed different shapes such as ovoid, pyramidal, fusiform at day 14. Compared with the Ti6Al4V/MSC, the Ti6Al4V/MSC/PRP group have more number and the morphology of MSCs were more similar to osteoblasts.

3.5 Implantation

3.5.1 Fluorescence analysis. All the animals recovered to normal after operation and reached the designated time point. No obvious postoperative complications were found. Interrupted fluorescent bone labeling and new bone deposition validated the bone remodeling. Markers were detected in the pores of the two groups in regenerated bone, indicating an increase in the rate of bone deposition into the pores of the scaffold (Fig. 5, tetracycline showed yellow, and calcein green showed green). Five measurements were made for each double labeled span of implanted and periprosthetic bone. The average thickness of the newly mineralized bone was then divided by

the 11 days marker interval and expressed in millimeter per day. At the 2nd, 8th and 12th week, the MAR of ingrowth bone was significantly higher than that of periprosthetic bone ($P < 0.05$) (Table 1). The MAR of bone ingrowth in MSC/PRP/Ti6Al4V group was significantly higher than that in the other two groups. MAR of MSC/PRP/Ti6Al4V group was higher than that of the other two groups at 8 and 12 weeks. MAR value of periprosthetic bone showed no significant difference among the three groups at each time point after operation ($P > 0.05$) (Table 1).

3.5.2 Histomorphometric analysis. The general tissue reaction among the groups was similar in Fig. 6. No osteoclast reaction was observed near the implants. In any case, no filtration was observed consisting of mononuclear cells. No filtration of neutrophils and eosinophils was observed, which indicated that the implants had good biocompatibility.[36] The bone tissue was red and the implant was black in the histological observation with toluidine blue staining. At 2 weeks after implantation, a small amount of new immature bone tissue grew from the edge of bone defect and began to directly deposit on the implant surface, and only minor bone grew into the external area [Fig. 6(a), (d) and (g)].

No debris or wear particles were found in the surrounding tissues. After 8 weeks, images indicated that bone formation progressed at the marginal area toward the center of the bone defect [Fig. 6(b), (e) and (h)]. In general, smaller pores are completely filled with bone, while the larger pores are partially filled. The bone formation of PRP group showed more bone-formation than that of other groups. At the 12th week, the trabecula was thicker than that at the 8th week, and formed new bone towards the center of the defect, which was connected with the edge of the wound.
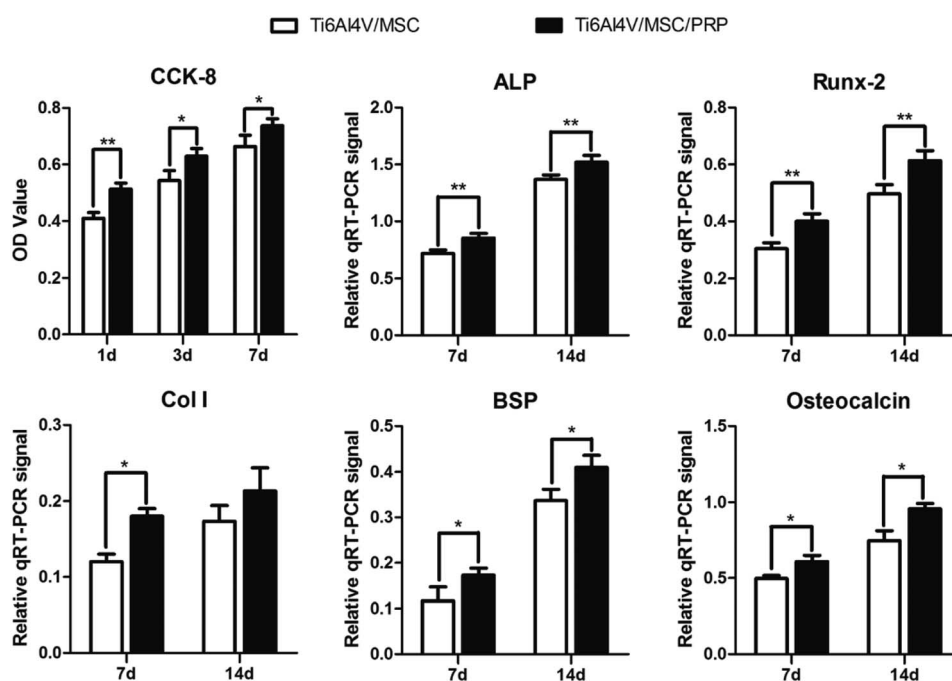

Fig. 4 The CCK-8 results of cell proliferation and the expression of ALP, Runx-2, Col I, BSP and osteocalcin in the Ti6Al4V/MSC group and Ti6Al4V/MSC/PRP group.
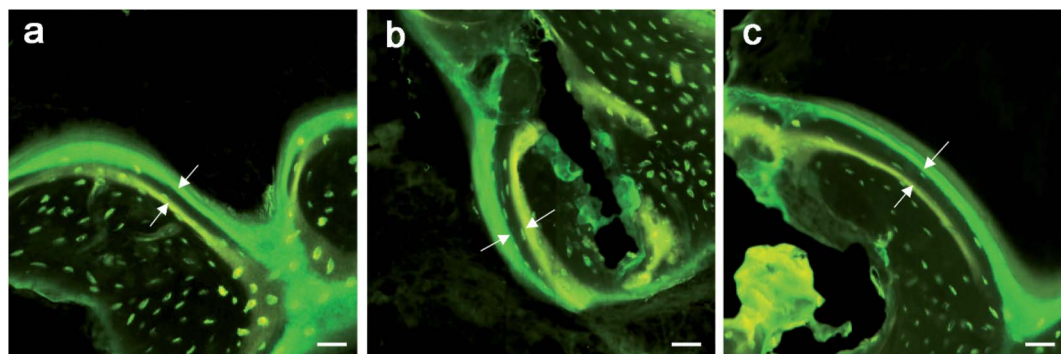
Fig. 5 Fluorescence images of the three groups: (a) bare porous Ti6Al4V scaffold, (b) Ti6Al4V/MSC and (c) Ti6Al4V/MSC/PRP group. Tetracycline labeling showed yellow and calcein green labeling showed green, the implant was in black color. Bone mineralization apposition rate is a vertical space between two markers interval (space between the white arrows). Scale bars represent 30 μm.

A lot of new bone was formed around the implant and osteoblasts were observed to arrange around the new bone. The newly formed bone has successfully bridged the bone defect [Fig. 6(c), (f) and (i)]. The process of bone remodeling can be seen in all implant sites. The osteogenesic rate of MSC/PRP/Ti6Al4V group was higher than that of the other two groups. Fig. 7a showed the quantitative data of BIC, and it was obvious that the extent of bone ingrowth in both groups increased significantly with time. However, the MSC/PRP/Ti6Al4V group had significantly higher BIC values than the other two groups at every time point. At 8 and 12 weeks, the Ti6Al4V/MSC group was significantly higher than the bare group.

3.6 Micro-CT analysis and push-out test

The micro-CT analysis confirmed that there were a lot of bone tissue and no obvious defect around the implant, and the interface between the bone tissue and the implant was well combined. This was also observed in the pores of porous samples at 8 and 12 weeks of each group. In Fig. 8, the images clearly show the integration of bone in the porous network in order to achieve better osseointegration.

Fig. 7b shows that the ingrowth bone volume of each group increased significantly from 2–12 weeks after operation ($P < 0.05$), and MSC/PRP/Ti6Al4V group was significantly higher than other groups at all time points ($P < 0.05$). In MSC/Ti6Al4V group, 8 and 12 weeks postoperatively, the interface shear strength (MPa) was significantly higher than that in the bare group ($P < 0.05$). At each time point, the interfacial shear strength of MSC/PRP/Ti6Al4V group was significantly higher

than that of the other two groups ($P < 0.05$), and the MSC/Ti6Al4V group was significantly higher than that of the bare group at 12 weeks ($P < 0.05$) (Fig. 7c).

4. Discussions

As a new biomaterial that have good osteoconductive ability, porous titanium scaffolds have attracted more and more attention in recent years.[38] In this study, porous titanium was prepared by a new powder sintering process. The implants with different porosities and pore sizes can be prepared by controlling the number and size of the intermediate particles added in Ti6Al4V powder. The binder used has the characteristics of clean decomposition, and there is no residue after sintering above 1200 °C, which is suitable for large-scale application cost and low pollution level. The microstructure and mechanical properties of implant are related to its pore size and porosity, which are the key parameters of implant life.[39] Studies have showed that high porosity and large pores were benefit to the bone ingrowth,[40,41] especially the porous materials with a porosity of 30–90% and pore size of 150–600 μm.[42] The results of micro-CT and SEM showed that the porous structure, three-dimensional connectivity, irregular pore shape and different sizes of the porous Ti6Al4V implant were similar to the natural cancellous bone.[43] The implant has high porosity of 76% with pore size larger than 500 μm. The mechanical test results showed that the material had high compressive strength and the elastic modulus of the implant (1.87 GPa) was close to that of the cancellous bone (0.5–2 GPa).[44] Therefore, the porous

Table 1 Mineralization apposition rates of the two groups[a]

	MAR of bone ingrowth (μm d^{-1})			MAR of periprosthetic bone (μm d^{-1})		
	Ti6Al4V	Ti6Al4V/MSC	Ti6Al4V/MSC/PRP	Ti6Al4V	Ti6Al4V/MSC	Ti6Al4V/MSC/PRP
2 weeks	3.04 ± 0.11	3.19 ± 0.15	3.36 ± 0.07	2.45 ± 0.24	2.59 ± 0.15	2.77 ± 0.19
8 weeks	2.58 ± 0.12	2.73 ± 0.08	2.92 ± 0.15	2.36 ± 0.12	2.41 ± 0.09	2.52 ± 0.21
12 weeks	2.34 ± 0.10	2.46 ± 0.13	2.61 ± 0.14	2.34 ± 0.14	2.36 ± 0.13	2.42 ± 0.16

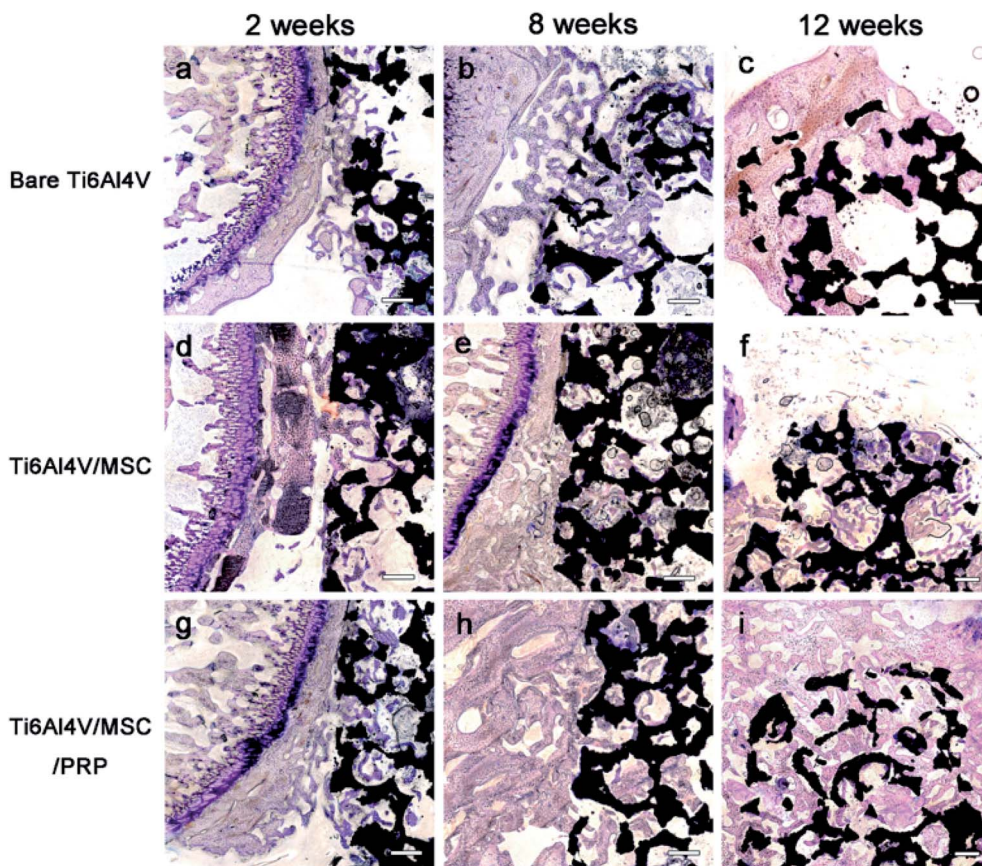[a] MAR, mineralization apposition rate.

Fig. 6 Histological results after implantation of 2, 8 and 12 weeks in the two groups with toluidine blue staining: (a–c) bare Ti6Al4V group, (d–f) Ti6Al4V/MSC group and (g–i) are the Ti6Al4V/MSC/PRP group. Scale bars represent 300 μm.

Ti6Al4V not only provides enough space for the growth of cells and bone, but also provides enough mechanical support in the process of bone growth without obvious stress shielding effect.

In recent years, many studies in regenerative medicine have used various biological factors to accelerate the process of bone healing, because growth factors can improve the biological activity of bone graft substitute.[45] PRP is an autogenous blood fraction with high platelet concentrations and various growth

factors, which has been widely used to enhance bone formation.[19,20] The cell adhesion molecule vitronectin which is required for osteoconduction and osteointegration is also rich in PRP.[46] In this study, the ELISA assay results showed a significantly higher level of growth factors existing in PRP than whole blood. The preparation method of the PRP can significantly influence the concentrations of platelets and growth factors,[47] and consequently their osteogenic capacity.[48] The current study
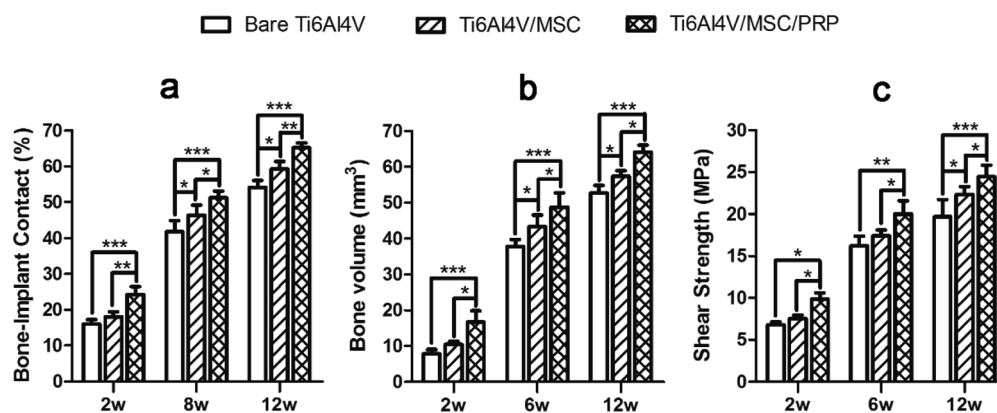

Fig. 7 The values of (a) bone-implant contact, (b) bone volume, and (c) shear strength in the two groups at 2, 8 and 12 weeks after implantation. * $P < 0.05$; ** $P < 0.01$.
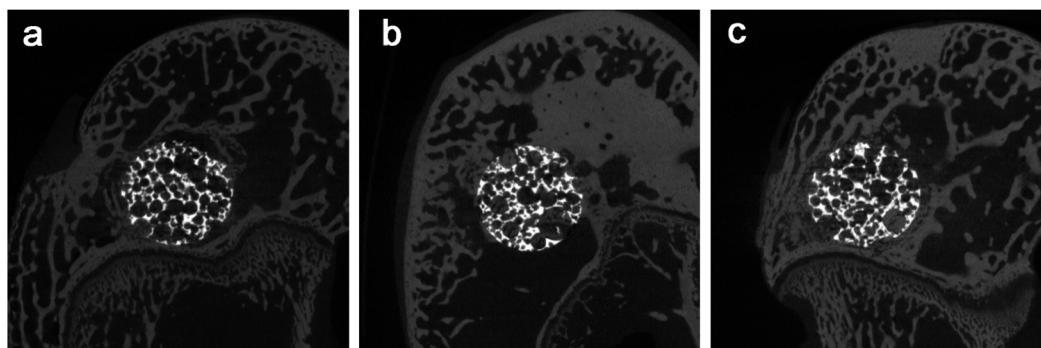
Fig. 8 The micro-CT images the two groups at 2 weeks after implantation: (a) the bare porous Ti6Al4V group (b) the Ti6Al4V/MSC group, and (c) the Ti6Al4V/MSC/PRP group.

acquired 5 to 12-fold platelets in PRP compared with whole blood by 2-step centrifugation procedure. A double centrifugation protocol has been shown to induce higher platelet concentrations when compared with single centrifugation protocols.[49] Another important parameter for PRP is the concentrations of platelets. Jagoda *et al.* demonstrated that different concentration of PRPs exerted different effects on the migration of human MSCs and umbilical-vein endothelial cells.[50] Notably, different kinds of seed cells may show discrepant responses to PRP stimulation. Xie *et al.* observed that same PRP gel exerted stronger pro-proliferative effects on bone marrow MSCs than adipose tissue-derived MSCs.[24] Therefore, it is necessary to determine the appropriate concentration of PRP for specific seed cells. Our previous study showed that the optimum platelet concentration for MSC osteogenesis may be 1500×10^9 pl per L, thus we used this concentration in the present work.

In this study, we first uniformly mixed PRP with MSCs in a liquid state and then after being mixed with thrombin and $CaCl_2$, we injected the PRP/MSCs complex into the porous Ti6Al4V scaffold.[51] By the catalytic action of thrombin and $CaCl_2$, PRP can form PRP gel.[18,52] The sol–gel transition of PRP can help encapsulate cells within the fibrin polymer easily, providing an ideal environment for bone mineralization.[53] Xie revealed that PRP matrix had a 3D mesh-like structure,[24] thus the PRP gel filled in the scaffold would not suppress the angiogenesis.[54] PRP gel can be produced simply without unnatural conditions and release abundant natural cytokines, thus we chose it as the delivery system. However, PRP gel often lacks the mechanical properties required for load-bearing applications. Therefore, in this study, we complicate the MSC/PRP with the porous Ti6Al4V for sufficient mechanical support.

The results of CCk-8 and live/dead tests indicated that the group with PRP had a higher cell proliferation than others at each time point. Cells with PRP grew better on the material surface and even grew deeply into the pores. Promoting cell proliferation of the porous biomaterials/PRP constructs are not only due to the 3D structures which simulate trabecular bone and support tissue ingrowth, but also to the large number of growth factors. In addition, the rough surface of porous Ti6Al4V may not only help in biological tissue attachment and cell

growth but also cause stronger degranulation and release of the growth factors from the platelets.[55] These results indicated the biocompatibility of the porous Ti6Al4V and PRP. The expression of genes and proteins related to bone growth and repair are important indicators of osteoblast phenotype *in vitro*. In the present work, after 7 and 14 days of incubation, the expression of bone growth related genes and proteins (ALP, Runx-2, Col I, BSP and osteocalcin) up-regulated in each group. The porous sample structure and PRP provide a larger and more suitable environment for the formation of bone-like tissues. Compared with other groups in this study and other studies, the porous Ti6Al4V/PRP structure extends the lifespan of osteoblasts and may extend their synthetic activity period, which eventually leads to an increase in the formation of bone tissue.[56]

However, because the *in vivo* environment is more complicated than the *in vitro* culture conditions, the good outcomes of experimental studies cannot guarantee the effectiveness for animals or humans. Therefore, we need an animal model to prove our experimental results. Previous studies have shown that the porous Ti6Al4V scaffold has bone conductivity due to its structure and interconnected pores, which can guide the surrounding bone tissue growth into and form new bone. Most importantly, Ti6Al4V/PRP/MSCs not only retains the bone conductivity of Ti6Al4V scaffolds, but also gives them the osteoinductive potential derived from the osteogenic ability of PRP and MSCs. In the present work, from the fluorescence and histomorphometric analysis, micro-CT images and push-out test results, direct adhesion (integration) of bone and implant, and the bone grows from the host bone bed to the implant are obviously observed as early as 2 weeks after surgery in each group. The penetration depth of the new bone increased with the implantation time, and the defect was finally healed after 12 weeks, indicating the good bone conductivity of porous implant. After long-term *in vivo* implantation, each group show a high degree of BIC and high-strength interfacial shear strength, indicating good osseointegration and the ability of bio-branching for the surrounding bone. Due to the combination of porous structure and solid matrix, the high endogenous value produces a stable structure and maintains mechanical strength. However, the PRP group showed significant faster bone growth speed, more bone ingrowth, and higher interfacial

strength at every point of implantation, especially in the first 2 weeks. The findings supported the hypothesis that the positive effects of PRP on bone grafts were seen in bone early healing and achieving early stability.[57] It is well known that platelets and growth factors play a role in the early stages of bone regeneration, but the lifespan of platelets and the direct effects of growth factors were as short as about 5 days. In the present work, results show that PRP still plays a positive role for the formation of new bone *in vivo* at 12 weeks after operation. In the clinical treatments for patients with implants, early stability, enhanced bone regeneration and reduced healing time after operation are critical, which can enable patients to earlier load and move autonomously for a faster rehabilitation, and avoid many bedridden risks, such as thrombosis and bedsore.

5. Conclusions

The porous Ti6Al4V/MSC/PRP construct showed good biocompatibility and osteogenic ability. The porous Ti6Al4V scaffolds incorporated with MSC and PRP may be more effective in enhancing the bone regeneration, and is expected to become an ideal material for biomaterials, especially bone defect repair and joint replacement.

Funding sources

Conflicts of interest

There are no conflicts to declare.

References

1 M. J. Yaszemski, R. G. Payne, W. C. Hayes, R. Langer and A. G. Mikos, *Biomaterials*, 1996, **17**, 175.

2 C. M. Court-Brown and M. M. Mcqueen, *J. Bone Jt. Surg., Am. Vol.*, 2016, **98**, e36.

3 D. I. Ilan and A. L. Ladd, *Operat. Tech. Plast. Reconstr. Surg.*, 2012, **28**, 457–468.

4 G. Lewis, *J. Mater. Sci.: Mater. Med.*, 2013, **24**, 2293–2325.

5 P. Heinl, L. Müller, C. Körner, R. F. Singer and F. A. Müller, *Acta Biomater.*, 2008, **4**, 1536–1544.

6 J. Parthasarathy, B. Starly, S. Raman and A. Christensen, *J. Mech. Behav. Biomed. Mater.*, 2010, **3**, 249–259.

7 A. Kumar, S. Mandal, S. Barui, R. Vasireddi, U. Gbureck, M. Gelinsky and B. Basu, *Mater. Sci. Eng., R*, 2016, **103**, 1–39.

8 D. S. J. Van, H. Wang, Y. S. Amin, M. Siebelt, M. Sandker, J. H. Waarsing, J. A. Verhaar, H. Jahr, A. A. Zadpoor and S. C. Leeuwenburgh, *Tissue Eng., Part A*, 2013, **19**, 2605–2614.

9 A. S. Brydone, D. Meek and S. Maclaine, *Proc. Inst. Mech. Eng., Part H*, 2010, **224**, 1329–1343.

10 F. Matassi, L. Nistri, D. C. Paez and M. Innocenti, *Clin. Cases Miner. Bone Metab.*, 2011, **8**, 21.

11 A. R. Gazdag, J. M. Lane, D. Glaser and R. A. Forster, *J. Am. Acad. Orthop. Surg.*, 1995, **3**, 1.

12 S. Gronthos, K. Stewart, S. E. Graves, S. Hay and P. J. Simmons, *J. Bone Miner. Res.*, 2010, **12**, 1189–1197.

13 S. Gronthos, S. E. Graves and P. J. Simmons, *Blood*, 1994, **84**, 4164.

14 S. Gronthos, S. Fitter, P. Diamond, P. J. Simmons, S. Itescu and A. C. Zannettino, *Stem Cells Dev.*, 2007, **16**, 953–963.

15 Z. L. Deng, K. A. Sharff, N. Tang, W. X. Song, J. Luo, X. Luo, J. Chen, E. Bennett, R. Reid and D. Manning, *Front. Biosci.*, 2008, **13**, 2001–2021.

16 P. Borrione, F. Fagnani, G. A. Di, A. Mancini, F. Pigozzi and Y. Pitsiladis, *Curr. Sports Med. Rep.*, 2017, **16**, 459.

17 F. Cimara Fortes, C. G. Márcia Cristina, F. José Scarso, G. José Mauro, O. S. E. Cláudia Maria and R. D. S. Magini, *Clin. Oral Implants Res.*, 2010, **16**, 456–460.

18 J. L. Drury and D. J. Mooney, *Biomaterials*, 2003, **24**, 4337–4351.

19 Y. H. Zhao, M. Zhang, N. X. Liu, X. Lv, J. Zhang, F. M. Chen and Y. J. Chen, *Biomaterials*, 2013, **34**, 5506–5520.

20 R. Landesberg, M. Roy and R. S. Glickman, *J. Oral Maxillofac. Surg.*, 2000, **58**, 297–300; discussion 300–291.

21 J. Zhu, B. Cai, Q. Ma, F. Chen and W. Wu, *J. Tissue Eng. Regener. Med.*, 2013, **7**, 819–830.

22 S. Huang, S. Jia, G. Liu, D. Fang and D. Zhang, *J. Oral Med. Oral Surg. Oral Pathol. Oral Radiol.*, 2012, **114**, S32–S40.

23 P. Kasten, J. Vogel, R. Luginbuhl, P. Niemeyer, S. Weiss, S. Schneider, M. Kramer, A. Leo and W. Richter, *Cells Tissues Organs*, 2006, **183**, 68–79.

24 X. Xie, Y. Wang, C. Zhao, S. Guo, S. Liu, W. Jia, R. S. Tuan and C. Zhang, *Biomaterials*, 2012, **33**, 7008–7018.

25 J. Zhang, B. A. Doll, E. J. Beckman and J. O. Hollinger, *J. Biomed. Mater. Res., Part A*, 2003, **67**, 389–400.

26 S. Mullens, I. Thijs, J. Cooymans and J. Luyten, *US Pat.*, US8992828, 2015.

27 J. Li, Z. L. Li, R. L. Li, Y. Y. Shi, H. R. Wang, Y. X. Wang and G. Jin, *RSC Adv.*, 2018, **8**, 36512–36520.

28 J. Li, Z. Li, Y. Shi, H. Wang, R. Li, J. Tu and G. Jin, *J. Mech. Behav. Biomed. Mater.*, 2018, **91**, 149–158.

29 J. Li, Z. Li, Q. Wang, Y. Shi, W. Li, Y. Fu and G. Jin, *RSC Adv.*, 2019, **9**, 1541–1550.

30 H. Zhu, X. X. Jiang, Z. K. Guo, H. Li, Y. F. Su, H. Y. Yao, X. Y. Wang, X. S. Li, Y. Wu, Y. L. Liu, Y. Zhang and N. Mao, *Stem Cells Dev.*, 2009, **18**, 1473–1484.

31 D. Li, Z. Heng, Y. Yang, W. Zhi-Dong, Z. Xiao-Li, Y. Hong-Min, D. Lei, Z. Hai-Hong, H. Dong-Mei and X. Mei, *Leuk. Lymphoma*, 2014, **55**, 1635–1644.

32 H. Zhu, Z. K. Guo, X. X. Jiang, H. Li, X. Y. Wang, H. Y. Yao, Y. Zhang and N. Mao, *Nat. Protoc.*, 2010, **5**, 550–560.

33 K. Wang, Z. Li, J. Li, W. Liao, Y. Qin and N. Zhang, *Tissue Eng., Part A*, 2019, **25**, 333–351.

34 B. M. Willie, X. Yang, N. H. Kelly, J. Merkow, S. Gagne, R. Ware, T. M. Wright and M. P. G. Bostrom, *J. Biomed. Mater. Res., Part B*, 2010, **92**, 479–488.

35 C. W. S. Ponader, M. Widenmayer, R. Lutz and P. Heinl, *J. Biomed. Mater. Res., Part A*, 2010, **92**, 56–62.

36 B. Chang, W. Song, T. Han, J. Yan, F. Li, L. Zhao, H. Kou and Y. Zhang, *Acta Biomater.*, 2016, **33**, 311–321.

37 F. Butz, T. Ogawa, T. L. Chang and I. Nishimura, *Int. J. Oral Maxillofac. Implants*, 2006, **21**, 687–695.

38 M. Niinomi and M. Nakai, *Int. J. Biomater.*, 2011, **2011**, 836587.

39 H.-C. Hsu, S.-K. Hsu, H.-K. Tsou, S.-C. Wu, T.-H. Lai and H. Wen-Fu, *J. Mater. Sci.: Mater. Med.*, 2013, **24**, 645–657.

40 Y. S. Amin, D. S. J. Van, Y. C. Chai, R. Wauthle, B. Z. Tahmasebi, P. Habibovic, M. Mulier, J. Schrooten, H. Weinans and A. A. Zadpoor, *Biomaterials*, 2014, **35**, 6172–6181.

41 W. Mróz, B. Budner, R. Syroka, K. Niedzielski, G. Golański, A. Slósarczyk, D. Schwarze and T. E. Douglas, *J. Biomed. Mater. Res., Part B*, 2015, **103**, 151–158.

42 D. Muller, H. Chim, A. Bader, M. Whiteman and J. T. Schantz, *Stem Cells Int.*, 2010, **2011**, 547247.

43 A. Syahrom, M. R. Abdul Kadir, J. Abdullah and A. Ö, *Med. Eng. Phys.*, 2013, **35**, 792–799.

44 D. Yang, H. Shao, Z. Guo, T. Lin and L. Fan, *Biomed. Mater.*, 2011, **6**, 045010.

45 J. J. de Obarrio, J. I. Araáz-Dutari, T. M. Chamberlain and A. Croston, *Int. J. Periodontics Restor. Dent.*, 2000, **20**, 486–497.

46 A. R. Sánchez, P. J. Sheridan and L. I. Kupp, *Int. J. Oral Maxillofac. Implants*, 2015, **18**, 93–103.

47 G. Weibrich, W. K. Kleis, G. Hafner, W. E. Hitzler and W. Wagner, *Clin. Oral Implants Res*, 2010, **14**, 357–362.

48 J. Wiltfang, F. R. Kloss, P. Kessler, E. Nkenke, S. Schultze-Mosgau, R. Zimmermann and K. A. Schlegel, *Clin. Oral Implants Res.*, 2004, **15**, 187–193.

49 M. J. H. Nagata, M. R. Messora, F. A. C. Furlaneto, S. E. Fucini, A. F. Bosco, V. G. Garcia, T. M. Deliberador and L. G. N. de Melo, *Eur. J. Dent.*, 2010, **4**, 395–402.

50 J. M. Jalowiec, M. D'Este, J. J. Bara, J. Denom, U. Menzel, M. Alini, S. Verrier and M. Herrmann, *Tissue Eng., Part C*, 2015, **22**, 229–230.

51 V. I. Sikavitsas, G. N. Bancroft and A. G. Mikos, *J. Biomed. Mater. Res.*, 2002, **62**, 136–148.

52 A. Mellati, C. M. Fan, A. Tamayol, N. Annabi, S. Dai, J. Bi, B. Jin, C. Xian, A. Khademhosseini and H. Zhang, *Biotechnol. Bioeng.*, 2017, **114**, 217–231.

53 S. Sahoo, J. G. Cho-Hong and T. Siew-Lok, *Biomed. Mater.*, 2007, **2**, 169–173.

54 M. Vishnu Priya, A. Sivshanmugam, A. R. Boccaccini, O. M. Goudouri, W. Sun, N. Hwang, S. Deepthi, S. V. Nair and R. Jayakumar, *Biomed. Mater.*, 2016, **11**, 035017.

55 J. P. M. Fennis, P. J. W. Stoelinga and J. A. Jansen, *Int. J. Oral Maxillofac. Surg.*, 2004, **33**, 48–55.

56 E. M. Lotz, R. Olivares-Navarrete, S. Berner, B. D. Boyan and Z. Schwartz, *J. Biomed. Mater. Res., Part A*, 2016, **104**, 3137–3148.

57 J. Han, H. X. Meng, J. M. Tang, S. L. Li, Y. Tang and Z. B. Chen, *Cell Proliferation*, 2007, **40**, 241–252.